Journal of
Materials Chemistry B

Accepted Manuscript

This article can be cited before page numbers have been issued, to do this please use: D. Li, Y. Zhang, S. Wen, Y. Song, Y. Tang, X. Zhu, M. Shen, S. Mignani, J. Majoral, Q. Zhao and X. Shi, *J. Mater. Chem. B*, 2016, DOI: 10.1039/C6TB00773B.

ROYAL SOCIETY OF CHEMISTRY

www.rsc.org/materialsB

Journal of Materials Chemistry B

View Article Online
DOI: 10.1039/C6TB00773B
PAPER

Cite this: DOI: 10.1039/c0xx00000x

www.rsc.org/xxxxxx

Construction of polydopamine-coated gold nanostars for CT imaging and enhanced photothermal therapy of tumors: an innovative theranostic strategy†

Du Li,[1a] Yongxing Zhang, [1b] Shihui Wen, [c] Yang Song, [c] Yueqin Tang, [d] Xiaoyue Zhu, [c] Mingwu Shen, [c] Serge Mignani, [e] Jean-Pierre Majoral, [f] Qinghua Zhao*[b] and Xiangyang Shi*[a,c]

Received (in XXX, XXX) Xth XXXXXXXXX 20XX, Accepted Xth XXXXXXXXX 20XX
DOI: 10.1039/b000000x

The advancement of biocompatible nanoplatforms with dual functionalities of diagnosis and therapeutics is strongly demanded in biomedicine in recent years. In this work, we report the synthesis and characterization of polydopamine (pD)-coated gold nanostars (Au NSs) for computed tomography (CT) imaging and enhanced photothermal therapy (PTT) of tumors. Au NSs were firstly formed *via* a seed-mediated growth method and then stabilized with thiolated polyethyleneimine (PEI-SH), followed by deposition of pD on their surface. The formed pD-coated Au NSs (Au-PEI@pD NSs) were well characterized. We show that the Au-PEI@pD NSs are able to convert the absorbed near-infrared laser light into heat, and have strong X-ray attenuation property. Due to the co-existence of Au NSs and the pD, the light to heat conversion efficiency of the NSs can be significantly enhanced. These very interesting properties allow their uses as a powerful theranostic nanoplatform for efficient CT imaging and enhanced phtotothermal therapy of cancer cells *in vitro* and the xenografted tumor model *in vivo*. With the easy functionalization nature enabled by the coated pD shell, the developed pD-coated Au NSs may be developed as a versatile nanoplatform for targeted CT imaging and PTT of different types of cancer.

Introduction

Recent advances in nanomedicine have prompted the development of multifunctional theranostic nanoplatforms that have integrated functionalities of tumor imaging and therapy within a single nanoparticulate system.[1-5] Taking advantage of the considerably improved physical, chemical, and biological characters, the multifunctional nanoplatforms can be rendered with capability of multimodal imaging as well as different forms of therapeutics.[5-9] Various imaging modalities, such as computed tomography (CT),[10-12] magnetic resonance (MR) imaging,[13, 14] fluorescence imaging,[15, 16] and positron emission tomography (PET)[17-19] could provide precise information for diagnosis of tumors. In particular, CT affords deep tissue penetration, better spatial and density resolution than other imaging modalities, and cost effectiveness.[20, 21] In addition, among the different strategies used for therapeutic treatments, photothermal therapy (PTT)[22-26] that is able to convert the near-infrared (NIR) laser light to heat, has been considered as one of the most effective approaches to suppress the tumor growth while minimizing the adverse side effects. Consequently, it is very important to develop a multifunctional theranostic nanomedicine platform for both CT imaging and PTT treatment of tumors.[27]

Recently, significant effort has been made to explore the development of gold nanoparticle (Au NP)-based nanoplatforms due to their outstanding optical attributes involving vigorous localized surface plasmon resonance (LSPR) absorption and scattering ability in the NIR region, and their ability for additional functionalization.[7] Typically, Au nanorods,[28-31] Au nanocages,[32-34] Au nanoshells,[35, 36] anisotropic Au NPs,[37-41] and Au nanostars (NSs)[38] are able to display LSPR in the NIR region. Among them, Au NSs with the highly branched structure show the higher photothermal transduction efficiency due to the easier penetration of the electric field.[39, 41, 42] In addition, Au NPs regardless of their shapes also possess better X-ray attenuation property than conventional iodine-based CT contrast agents (e.g., Omnipaque).[8, 10] Therefore, Au NSs may be used as a theranostic nanoplatform for CT imaging and PTT of tumors thanks to the NIR absorption property. For instance, Liu *et al.* demonstrated that Au NSs-based probe could be used for multi-modality imaging (including surface-enhanced Raman scattering, CT, and two-photon luminescence imaging) and PTT of tumors.[43] Gu and coworkers[42] modified uniform Au NSs with targeting ligands cyclic RGD peptide and anti-cancer drug doxorubicin to obtain a multifunctional nanoconstruct for targeted tumor imaging and combined PTT and chemotherapy of tumors. However, little effort was attempted to improve the PTT performance of the Au NSs.

Dopamine (DA),[44, 45] a neurotransmitter, plays a central role in the working of the brain's built-in reward circuit, and is also a small-molecule mimic of the adhesive proteins of mussels. Under alkaline pH and oxidative conditions, DA can be self-polymerized to form polydopamine (pD), that can be deposited onto different surfaces.[46-48] In addition, pD is chemically stable and biocompatible,[47, 48] allowing for their uses in various biomedical applications as a nature-inspired polymer. Furthermore, the high density of functional groups of pD, such as catechol and amine, are beneficial for enhanced attachment of diverse biomolecules.[48, 49] Importantly, pD has been applied for

PTT of tumors *in vivo* due to its prominent NIR absorption feature that enables effective photothermal conversion.[47, 48, 50] Although both Au NPs with a specific shape (e.g. Au NSs) and pD display NIR absorption features, to our knowledge, currently there is no combination of both Au NSs and pD within one single nanoplatform for CT imaging and enhanced PTT of tumors.

With the aim to develop a novel nanoplatform for both CT imaging and enhanced PTT of tumors, in this work we attempted to prepare Au NSs coated with pD. As shown in Figure 1, Au NSs were prepared by seed-growth method, stabilized by partially thiolated polyethyleneimine (PEI-SH), followed by pD shell coating onto their surface *via in situ* polymerization of DA. The fabricated Au-PEI@pD NSs were thoroughly characterized by several analytical techniques. Their stability, cytocompatibility, X-ray attenuation property, and ability to be used for CT imaging of cancer cells *in vitro* and *in vivo* were then investigated. Likewise, the enhanced photothermal conversion efficiency of the Au NSs and the use of the Au NSs for PTT of cancer cells *in vitro* and *in vivo* were also evaluated. To our knowledge, this is the first report related to the development of pD-coated Au NSs for CT imaging and enhanced PTT of tumors.

Experimental

Materials

Branched PEI (Mw = 25 000) and dopamine hydrochloride were supplied by Aldrich (St. Louis, MO). 1-Ethyl-3-(3-(dimethylamino)propyl) carbodiimide hydrochloride (EDC), Tris (hydroxymethyl) aminomethane, N-hydroxysuccinimide (NHS), mercaptoacetic acid (MA) and 3-(4,5-dimethylthiazol-2-yl)-2,5-diphenyltetrazolium bromide (MTT) were obtained from TCI (Tokyo, Japan). $HAuCl_4 \cdot 4H_2O$, $AgNO_3$, trisodium citrate and ascorbic acid (AA) were purchased from Sinopharm Chemical Reagent Co., Ltd. (Shanghai, China). HeLa cells (a cervical carcinoma cell line) were acquired from Institute of Biochemistry and Cell Biology, the Chinese Academy of Sciences (Shanghai, China). Fetal bovine serum (FBS), Dulbecco's modified Eagle's medium (DMEM), Penicillin and streptomycin were from HyClone Lab., Inc. (Logan, UT). Water used in all experiment was filtered *via* a Milli-Q Plus 185 water purification system (Millipore, Bedford, MA). Cellulose dialysis membranes (molecular weight cut-off, MWCO = 8000-14000) was procured from Shanghai Chaoyan Biotechnology Co., Ltd. (Shanghai, China).

Synthesis of partially thiolated PEI

MA (13.8 μL, 100 molar equiv. of PEI) dissolved in 20 mL water was firstly activated by EDC (100.0 mg)/NHS (52.2 mg) with 2.5 molar equiv. of MA for 3 h, then the activated MA was dropwise added to PEI aqueous solution (15 mL, 50.0 mg) under continuous magnetic stirring. After 24 h, the reaction mixture was dialyzed against phosphate buffered saline (PBS) and water (each for 5 times, 2L) using a dialysis membrane with an MWCO of 8000-14000 for 3 days, followed by lyophilization to acquire the PEI-SH product.

Synthesis of PEI-coated AuNSs

Au NSs were synthesized *via* seed-mediated growth method according to a previous report with some slight adjustments.[39] Typically, Au seeds were formed by dropping 1% trisodium citrate (1.5 mL) into a boiling solution of $HAuCl_4$ (10 mL, 1 mM) under vigorous stirring for 10 min. After cooling down to room temperature, the solution was filtered with cellulose membrane with a pore size of 0.22 μm. Then, the Au NSs were synthesized by instantaneously mixing percolated Au seeds (100 μL), $AgNO_3$ (100 μL, 3 mM), AA (50 μL, 0.1 M), and $HAuCl_4$ (10 mL, 0.25 mM) with vigorous stirring for 1 min.

Afterward, Au NSs were modified with PEI by adding PEI-SH (5.86 mg, 10 molar equiv. of Au NSs) into the above aqueous solution of Au NSs. The mixture solution was continuously stirred for 24 h, then the obtained PEI-modified Au NSs (AuNSs-PEI) were collected through 3 cycles of centrifugation/redispersion in water. The formed AuNSs-PEI were redispersed in water (10 mL) for further use.

Formation of Au-PEI@pD NSs

In order to coat a thin pD shell onto the surface of the AuNSs-PEI, the AuNSs-PEI suspension was incubated in 50 mL of Tris buffer solution (10 mM, pH 8.5) containing 6 mg DA. After shaking at room temperature for 4 h, Au-PEI@pD NSs were formed and purified by virtue of centrifugation (6 000 rpm, 8 min) and rinsing with water for 3 times. The final Au-PEI@pD NSs were resuspended in water before characterization and use.

Characterization techniques

UV-vis spectrometry, fourier transform infrared (FTIR), transmission electron microscopy (TEM), thermal gravimetric analysis (TGA), and dynamic light scattering (DLS) were used to characterize the formed Au-PEI@pD NSs. A detailed experimental procedure can be found in our previous work.[5] CT imaging of Au-PEI@pD NSs with different Au concentrations was performed using a GE LightSpeed VCT imaging system with 100 kV, 80 mA, and a slice thickness of 0.625 mm. The Au-PEI@pD NSs were irradiated with an 808 nm laser (1.3W/cm^2, laser power was 81 mW and beam spot size was 0.0625 cm^2) and the temperature of the solution was tracked by a DT-8891E thermocouple linked to a digital thermometer (Shenzhen Everbest Machinery Industry, Shenzhen, China).

Cell viability assay

HeLa cells were regularly cultured in DMEM supplemented with 10% FBS and 1% penicillin (100 units/mL)/streptomycin (100 μg/mL) in a 37 ^oC incubator with 5% CO_2. MTT assay of HeLa cells was performed to test the cytotoxicity of Au-PEI@pD NSs according to our reported protocols.[13]

CT imaging of cancer cells *in vitro*

HeLa cells seeded in 25 cm^2 canted culture flask at a density of 1 × 10^6 per flask were brought to confluence after 24 h incubation at 37 ^oC and 5% CO_2. Then the medium was replaced with 5 mL of fresh medium containing the Au-PEI@pD NSs at different Au concentrations (0, 3.125, 6.25, 12.5, 25, and 50 μM, respectively) and the cells were cultured for another 4 h. After that, the cells were washed, trypsinized, resuspended in 0.1 mL PBS, and placed in 1.5-mL Eppendorf tubes before CT imaging. CT scanning was performed *via* GE LightSpeed VCT imaging system using parameters similar to those used in the CT phantom studies.

CT imaging of a xenografted tumor model *in vivo*

The entire animal experiments were completed under the guidelines of the institutional committee for animal care and the instruction of the National Ministry of Health. The xenografted tumor model were established in the right flank back of male BALB/c nude mice (15-20 g). When the tumor nodules reached a suitable size (0.5-1.0 cm^3), the tumor-bearing mice were intratumorally injected with the Au-PEI@pD NSs ([Au] = 100 mM, in 100 μL PBS). CT scans were carried out before and at 10

min postinjection of the particles using the same instrumental parameters as described above.

PTT of cancer cells *in vitro*

HeLa cells were incubated with Au-PEI@pD NSs at different Au concentrations (0, 0.35, 0.7, 1.4, and 2.1 mM, respectively), then irradiated by an 808 nm laser with a power density of 1.3 W/cm^2. The PTT effects of cells were confirmed by MTT cell viability assay and cell morphology observation *via* a Leica DM IL LED inverted phase contrast microscope, respectively, according to our previous work.[5]

PTT of a xenografted tumor model *in vivo*

Sixteen HeLa tumor-bearing nude mice were randomly assigned to four groups. The mice in Control group were intratumorally injected with PBS (0.1 mL) without laser irradiation; mice in the Laser group were injected with PBS (0.1 mL) and each tumor site was subsequently exposed to an 808 nm laser for 10 min (power density = 1.3 W/cm^2); mice in the NSs group were treated with the Au-PEI@pD NSs ([Au] = 5.6 mM, in 0.1 mL PBS) without laser irradiation; and mice in the NSs + Laser group were treated with the Au-PEI@pD NSs ([Au] = 5.6 mM, in 0.1 mL PBS), followed by irradiation with an 808 nm laser (power density = 1.3 W/cm^2) for 10 min. The tumor size, body weight, and survival rate of all mice were measured and photographs of mice were taken at different time points. The tumor volumes were gauged and calculated using the following formula: (tumor length × (tumor width)^2)/2, and the survival rate of each group of mice was computed using the formula of N1/N × 100%, where N1 and N represent the amount of surviving mice and the sum of all mice in each group, respectively.

Histological examinations

Hematoxylin and eosin (H&E) and TdT-mediated dUTP Nick-End Labeling (TUNEL) staining of tumor sections were performed according to protocols described in the literature.[9]

Statistical analysis

The significance of the PTT treatment results were conducted *via* one-way analysis of variance (ANOVA) statistical analysis previously depicted in our work.[5] A p value of 0.05 was regarded as the significance level, and the data were labeled as (*) for $p < 0.05$, (**) for $p < 0.01$, (***) for $p < 0.001$, respectively. Some more experimental details are described in Electronic Supplementary Information (ESI).

Results and discussion

Synthesis and characterization of Au-PEI@pD NSs

In order to synthesize Au-PEI@pD NSs for theranostic applications, Au NSs were first synthesized with a seed-mediated growth approach,[39] stabilized by PEI *via* modification of the NSs with PEI-SH, and finally coated with a pD shell by self-polymerization of DA in order to have improved photothermal efficiency (Figure 1).

First, Au seed particles with a mean diameter of 13.6 nm (Figure S1a-b, ESI) were produced by reducing boiling $HAuCl_4$ with trisodium citrate. The Au seeds with a deep wine red solution color have an apparent SPR peak at around 520 nm (Figure 2a). Thereafter, the formed Au seeds were exposed to the Au growth solution in the presence of $AgNO_3$, leading to the formation of Au NSs. To render the Au NSs with sufficient colloidal stability, the Au NSs were further modified with PEI-SH *via* an approach reported in our previous work.[5] The formed PEI-modified Au NSs have a mean diameter of 72.3 ± 16.4 nm with a quite narrow size distribution (Figure S1c-d). Followed by self-polymerization of DA in the presence of the PEI-modified Au NSs, pD coating onto the Au NSs was achieved.

View Article Online
DOI: 10.1039/C6TB00773B

FTIR spectroscopy was used to confirm the coating of PEI and pD onto the surface of Au NSs (Figure S2, ESI). The band emerging at 1635 cm^{-1} for Au NSs could be ascribed to the appearance of OH^-, H_2O and oxidized products of citrate in the process of citrate reduction of Au salt. By comparison with the FTIR spectrum of PEI-SH, an enhanced peak emerging at about 1640 cm^{-1} in the spectrum of the AuNSs-PEI can be ascribed to the PEI amide linkage (vibration of C=N), suggesting that PEI-SH has been successfully modified onto the surface of Au NSs. The spectrum of dopamine is characterized by skeletal vibration of aromatic double bonds (1650–1400 cm^{-1}), stretching ν(C–O) of the catechol moieties appearing at 1283 cm^{-1}, in-plane bending of (C–H) at 1170 cm^{-1} and stretching ν(C–C–N) of the aminoethyl chains at 935 cm^{-1}.[51] After pD deposition onto the surface of the AuNSs-PEI, another four characteristic dopamine peaks at 1600 cm^{-1}, 1580 cm^{-1}, 1500 cm^{-1}, and 1450 cm^{-1} originated from the C=C vibrations of aromatic bonds still existed, whereas the prominent peak at 1650 cm^{-1} verified the formation of quinone groups of pD, thus indicating a confluent adherention of pD shell onto the AuNSs-PEI, in agreement with the literature.[51-53]

After the Au growth, the Au-PEI@pD NSs exhibit a blue solution color and noticeable SPR peak at 726 nm (Figure 2b), which is suitable for PTT of tumors using NIR laser irradiation. The morphology and size of the Au-PEI@pD NSs were characterized by TEM (Figure 2c,f). As visualized in Figure 2c, Au-PEI@pD NSs possess a star shape with a quite uniform size distribution, and the average diameter of the NSs (without the pD shell) was estimated to be 74.2 ± 15.0 nm, approximately similar to that before pD deposition (Figure S1d, ESI). TEM image also shows that a transparent shell appears on the surface of the Au NSs with a shell thickness of about 18 nm, further confirming the success of the pD deposition (Figure 2f). In contrast, the Au NSs modified with PEI without further pD deposition do not display such an apparent polymer shell (Figure 2e). It should be noted that the thickness of the pD shell can be controlled by tuning the concentration of dopamine and the polymerization time.[54, 55] In our case, the pD coating with a thickness of 18 nm is sufficient to prove the enhanced PTT efficiency of Au NSs (see below).

Zeta potential measurements were further carried out to validate the successful surface functionalization of the Au NSs. AuNSs-PEI dispersed in water have a positive potential (+49.8 mV) due to the surface modification of PEI-SH with abundant amines. After formation of pD shell, the zeta potential of the NSs changes from positive to negative (-17.3 mV), signifying the successful deposition of pD.[48] Likewise, the hydrodynamic size of the AuNSs-PEI changes from 90.5 nm to 125.8 nm after pD deposition (Figure S6a, ESI). The enlarged periphery of the Au-PEI@pD NSs should be attributed to the pD coating.

The Au content in the Au-PEI@pD NSs was measured by ICP-OES, and the result shows that the percentage of Au within the composite NSs is 82%. The PEI modification and subsequent pD deposition onto the surface of Au NSs were also confirmed by TGA (Figure S3, ESI). In comparison with unmodified Au NSs having a weight loss of 1.1% at 700 °C, the PEI modification endows the NSs with a weight loss of 3.5%. Further pD deposition gives rise to an increased weight loss of 18.1% for the Au-PEI@pD NSs. Therefore, the percentages of PEI and pD modifications were estimated to be 2.4% and 15.6%, respectively.

Overall, the organic content of the final Au-PEI@pD NSs was 18%, corroborating the ICP-OES data. The colloidal stability of the Au-PEI@pD NSs was evaluated by exposing them to water and compared with the uncoated Au NSs, AuNSs-PEI, and AuNSs@pD (Figure S4, ESI). It appears that uncoated Au NSs and AuNSs@pD without the PEI-SH are not stable and precipitation occurs during the experimental time period. In contrast, Au NSs coated with PEI and further deposited with pD are quite colloidally stable for at least 7 days. In this case, PEI-SH is essential to pre-stabilize the Au NSs through formation of Au-S bond before pD coating. Compared with the spectra of AuNSs-PEI dispersed in water (Figure S5a), the Au-PEI@pD NSs show an enhanced the SPR absorption, suggesting that the pD coating likely contributes to the enhanced PTT effect. Although the aminated PEI shows distinct cytotoxicity to cells, the further pD coating is able to render the particles with good cytocompatibility (see below). Furthermore, our data also show that the Au-PEI@pD NSs do not display apparent spectral changes after exposed to either saline or PBS buffer for at least 7 days (Figure S5b). The colloidal stability of the Au-PEI@pD NSs in water and PBS was further monitored by measuring their hydrodynamic size (Figure S6, Electronic Supplementary Information). We show that the hydrodynamic size of the Au-PEI@pD NSs does not have any significant changes within 7 days, further demonstrating their good stability.

Cytotoxicity assay

Before theranostic application of the developed Au-PEI@pD NSs, the cytotoxicity of AuNSs-PEI and Au-PEI@pD NSs were first evaluated by standard MTT viability assay of HeLa cells (Figure S7, ESI). Clearly, when compared to the cells treated with PBS ([Au] = 0 mg/mL), no significant cytotoxicity of the Au-PEI@pD NSs is discovered even at the Au concentration of the particles as high as 0.41 mg/mL, while the cells treated with the AuNSs-PEI at the same concentration display an apparently lower viability than those treated with the Au-PEI@pD NSs. Accordingly, we can safely claim that the developed Au-PEI@pD NSs have a good cytocompatibility in the given Au concentration range, which is crucial for their further biomedical explorations.

CT imaging of cancer cells *in vitro* and *in vivo*

The possibility to adopt Au-PEI@pD NSs as a CT contrast agent was next validated by X-ray attenuation intensity evaluation (Figure 3a-b). Due to the fact that the atomic number of Au is much higher than that of iodine, which is the radiodense element of conventional CT contrast agents (e.g., Omnipaque), Au NPs always display a better X-ray attenuation property than Omnipaque.[10] In our study, it can be seen that the brightness of the CT phantom images of the Au-PEI@pD NSs augments with the Au concentration (0.01-0.08 M), correlating well with the quantitative CT value change of the Au-PEI@pD NSs as a function of Au concentration.

To investigate the effectiveness to utilize the Au-PEI@pD NSs for CT imaging of cancer cells, CT images of cells incubated with the NSs at various Au concentrations were recorded (Figure 3c-d). It can be seen that the brightness of the CT images of HeLa cells increases with the increase of the Au concentration (Figure 3c). This is consistent with the change of the quantified CT value of cells as a function of Au concentration. The capability of the Au NSs for CT imaging of cancer cells could be due to the fact that the NSs are able to be uptake by cells through two distinct mechanisms (phagocytosis and diffusion *via* cell walls), in agreement with the literature.[10]

Next, we evaluated the potential to use the Au-PEI@pD NSs as a contrast agent for CT imaging of a xenografted tumor model *in vivo* (Figure 3e). After intratumoral injection of the Au-PEI@pD NSs, tumor region is enlightened at 10 min postinjection in the CT image. The CT values of the tumor region before and at 10 min postinjection were quantified to further delineate the CT contrast enhancement. The CT value in the tumor region before injection is 37.5 HU, while at 10 min postinjection the tumor CT value dramatically increases to 424.3 HU. These results suggest that the acquired Au-PEI@pD NSs have a promising capability for *in vivo* tumor CT imaging.

Photothermal property of the Au-PEI@pD NSs

The strong LSPR absorption peak of the Au-PEI@pD NSs in the NIR region motivated us to study their photothermal property (Figure 4). Both AuNSs-PEI and Au-PEI@pD NSs with the same Au concentration (0.35 mM) were exposed to an 808 nm laser for 300 s at a power density of 1.3 W/cm^2, and the temperature was monitored (Figure 4a). Under the same Au concentration, Au-PEI@pD NSs display a more prominent temperature increase than AuNSs-PEI, confirming the role played by the deposited pD to enhance the photothermal property of the particles due to its prominent NIR absorption feature and high photothermal conversion efficiency (40%).[50] The solution temperature of the Au-PEI@pD NSs increases from 25.1 to 40.2 ºC, while that of the AuNSs-PEI only increases from 24.7 to 35.2 ºC in the same time frame of 300 s (Figure 4a). The solution temperature increment of the Au-PEI@pD NSs is 1.4 times higher than that of the AuNSs-PEI within a time period of 300 s. The 808 nm laser photothermal conversion efficiency (Η) of the Au-PEI@pD NSs was calculated to be 49.9% according to the literature,[56, 57] which is higher than that of the AuNSs-PEI (36.1%) without pD coating. It should be noted that although the Au-PEI@pD NSs display an SPR peak at 726 nm, we can still use an 808 nm laser for heat generation due to the broad NIR absorption ranging from 600 nm to 900 nm. Further optimization of the synthesis parameters to get Au NSs with an SPR peak at 808 nm is necessary to achieve the maximum photothermal conversion efficiency.

The Au-PEI@pD NSs also display an Au concentration-dependent photothermal property (Figure 4b). With the increase of Au concentration, the solution temperature of the NSs increases more significantly under the laser irradiation. The solution temperature of the Au-PEI@pD NSs at an Au concentration of 2.1 mM increases from 25.6 to 51.1 ºC after 300 s laser irradiation, while water experiences a temperature increase of 2.7 ºC under the same condition. With the increase of Au concentration from 0.35 to 0.7, 1.4, 2.1 mM, the aqueous suspension of the Au-PEI@pD NSs showed a temperature increase of 15.1, 19.7, 23.2, and 25.5 ºC, respectively (Figure 4c). Moreover, the Au-PEI@pD NSs also exhibit a robust photothermal stability even after three cycles of NIR laser irradiation (808 nm laser at 1.3 W/cm^2, 300 s laser irradiation for each cycle, Figure 4d). Clearly, our results demonstrated that the developed Au-PEI@pD NSs displayed an excellent photothermal property, which is essential for their applications in PTT of tumors.

Photothermal ablation of cancer cells *in vitro* and a tumor model *in vivo*

The effective photothermal conversion efficiency of the Au-PEI@pD NSs inspired us to inspect their potential for photothermal ablation of cancer cells *in vitro* (Figure S8, ESI) and a xenografted tumor model *in vivo*. Qualitative cell morphology observation reveals that HeLa cells treated with laser alone display similar attachment morphology to the PBS control

(Figure S8a-b), indicating that the treatment of laser alone does not exert any damage to the cancer cells. In contrast, most of the HeLa cells incubated with the Au-PEI@pD NSs and then irradiated with an 808 nm laser for 5 min are dead, and only a small fraction of cells adheres to the plate after washing (Figure S8c-f). With the increase of Au concentration, the fraction of healthy cells is getting smaller.

Quantitative MTT cell viability assay was also used to confirm the efficacy of the Au-PEI@pD NSs for ablation of cancer cells (Figure S8g-h). Clearly, the viability of HeLa cells treated with the Au-PEI@pD NSs plus laser irradiation is significantly decreased even at the Au concentration as low as 0.07 mg/mL ($p < 0.05$) and the cell viability reaches minimum (48.6%) at an Au concentration of 0.41 mg/mL. Similar to the cell morphology observation data, the viability of cells after treatment with laser alone does not seem to have a change when compared to the PBS control. Taken together, our results show that the developed Au-PEI@pD NSs are able to effectively ablate cancer cells with the assistance of laser irradiation.

We next examined the capability of the Au-PEI@pD NSs for photothermal imaging and PTT of a xenografted tumor model *in vivo*. HeLa tumor-bearing mice were intratumorally injected with 0.1 mL PBS or 0.1 mL PBS containing the Au-PEI@pD NSs ([Au] = 5.6 mM), respectively, followed by laser irradiation for 5 min (Figure 5a-b). Note that we used intratumoral injection to complete the PTT of tumors, just because the tumor region has much more particle accumulation using this injection route than other injection routes (e.g., intravenous injection), in agreement with the study performed by Langer *et al*.[58] Only a modest temperature change is shown in the tumor region injected with PBS (Figure 5a), whereas the tumor region injected with the Au-PEI@pD NSs display an apparent temperature increase from 29.8 to 58.7 ºC within 300 s (Figure 5c). Our data indicate that the developed Au-PEI@pD NSs are able to be used for *in vivo* thermal imaging of the tumor region.

The potency to use the Au-PEI@pD NSs for PTT of tumors was next investigated by gauging the tumor size after different treatments (Figure 6a). The tumors treated with laser and NSs alone display a similar growth rate to the control group injected with PBS, illustrating that neither laser nor the Au-PEI@pD NSs alone is able to inhibit the tumor growth. In remarkable contrast, the tumors treated with NSs plus laser are able to be completely ablated at 20 days posttreatment. This can also be confirmed by taking pictures of mice at different days posttreatment (Figure S9, ESI). Furthermore, mice under varying treatments can well maintain their body weights during the period of *in vivo* experiments (Figure 6b), implying that the treatments of laser alone, Au-PEI@pD NSs alone, and the Au-PEI@pD NSs plus laser do not seem to damage the mice or be toxic to the mice. The PTT efficiency of tumors was further evaluated by recording the survival rate of the mice after different treatments. We can see that mice treated with the Au-PEI@pD NSs plus laser present a 100% survival rate within 60 days (Figure 6c), which is significantly higher than those in the groups of Control (0%), NSs (0%), and Laser (25%). Our results suggest that the formed Au-PEI@pD NSs can be used as a powerful platform for PTT of tumors.

H&E and TUNEL staining

The PTT efficacy of tumors using the developed Au-PEI@pD NSs was further evaluated by H&E and TUNEL staining of tumor sections. The micrographs of H&E-stained tumor slices (Figure 7a) reveal that the tumors treated with laser or Au-PEI@pD NSs alone exhibit the regular shape of tumor cells, similar to those treated with PBS (Control). In contrast, tumors treated with the NSs plus laser display necrosis cells in the whole section. Likewise, the effect of photothermal ablation of tumors was also evaluated by TUNEL staining (Figure 7b). It is evident that only rare positive staining of apoptotic cells emerge in the groups of Control, Laser, or NSs groups. In contrast, a significant amount of positively stained apoptotic cells appears in the section of tumors treated with the Au-PEI@pD NSs plus laser irradiation (Figure 7b). Finally, the apoptosis rates of the tumors were quantified by analysis of the TUNEL stained sections (Figure S10, ESI). The percentage of apoptotic cells follows the order of Control (6.9%) < NSs (8.2%) < Laser (18.3%) < NSs + Laser (86%).

Conclusion

In summary, we designed and synthesized Au-PEI@pD NSs as an innovative theranostic nanoplatform for CT imaging and enhanced PTT of tumors. The Au NSs firstly produced with a seed-mediated growth method can be easily modified with PEI, followed by deposition of pD to render the NSs with enhanced photothermal property. The constructed Au-PEI@pD NSs are water dispersible, colloidally stable, and non-toxic in the studied concentration range. Importantly, the designed Au-PEI@pD NSs are able to be applied as a powerful theranostic nanoplatform for in vivo CT imaging and enhanced PTT of tumors. Due to the easy functionalization of the deposited pD shell, it is expected that multifunctional pD-coated Au NSs may be developed as a versatile platform for targeted CT imaging and PTT of different types of cancer.

Acknowledgements

This research is financially supported by the National Natural Science Foundation of China (21273032 and 21405012), the Program for Professor of Special Appointment (Eastern Scholar) at Shanghai Institutions of Higher Learning, the Science and Technology Commission of Shanghai Municipality (15520711400). X. Zhu gratefully acknowledges the support from Shanghai Pujiang Program (14PJ1400400). M. Shen and X. Zhu thank the financial support from the Fundamental Research Funds for the Central Universities. D. Li thanks the support from the Chinese Universities Scientific Fund (CUSF-DH-D-2016034).

Notes and references

[a] *State Key Laboratory for Modification of Chemical Fibers and Polymer Materials, College of Materials Science and Engineering, Donghua University, Shanghai 201620, People's Republic of China*
[b] *Department of Orthopaedics, Shanghai General Hospital, School of Medicine, Shanghai Jiaotong University, Shanghai 200080, People's Republic of China. E-mail: sawboneszhao@163.com*
[c] *College of Chemistry, Chemical Engineering and Biotechnology, Donghua University, Shanghai 201620, People's Republic of China. E-mail: xshi@dhu.edu.cn*
[d] *Experiment Center, Shanghai General Hospital, School of Medicine, Shanghai Jiaotong University, Shanghai 200080, People's Republic of China*
[e] *PRES Sorbonne Paris Cité, CNRS UMR 860, Laboratoire de Chimie et de Biochimie pharmacologiques et toxicologique, Université Paris Descartes, 45, rue des Saints Pères, 75006, Paris, France*
[f] *Laboratoire de Chimie de Coordination du CNRS, 205 route de Narbonne, BP 44099, F-31077 Toulouse Cedex 4, France*

[1] *Du Li and Yongxing Zhang contributed equally to this work.*

† **Electronic supplementary information (ESI) available**: additional experimental results.

1. K. Y. Choi, G. Liu, S. Lee and X. Chen, *Nanoscale*, 2012, **4**, 330-342.
2. H. Dong, S.-R. Du, X.-Y. Zheng, G.-M. Lyu, L.-D. Sun, L.-D. Li, P.-Z. Zhang, C. Zhang and C.-H. Yan, *Chem. Rev.*, 2015, **115**, 10725–10815.
3. R. Kumar, W. S. Shin, K. Sunwoo, W. Y. Kim, S. Koo, S. Bhuniya and J. S. Kim, *Chem. Soc. Rev.*, 2015, **44**, 6670-6683.
4. N. Lee, D. Yoo, D. Ling, M. H. Cho, T. Hyeon and J. Cheon, *Chem. Rev.*, 2015, **115**, 10637–10689.
5. J. Li, Y. Hu, J. Yang, P. Wei, W. Sun, M. Shen, G. Zhang and X. Shi, *Biomaterials*, 2015, **38**, 10-21.
6. M. Elsabahy, G. S. Heo, S.-M. Lim, G. Sun and K. L. Wooley, *Chem. Rev.*, 2015, **115**, 10967–11011.
7. J. A. Webb and R. Bardhan, *Nanoscale*, 2014, **6**, 2502-2530.
8. D. Li, S. Wen and X. Shi, *Wiley Interdiscip. Rev.: Nanomed. Nanobiotechnol.*, 2015, **7**, 678-690.
9. J. Zhu, L. Zheng, S. Wen, Y. Tang, M. Shen, G. Zhang and X. Shi, *Biomaterials*, 2014, **35**, 7635-7646.
10. C. Peng, L. Zheng, Q. Chen, M. Shen, R. Guo, H. Wang, X. Cao, G. Zhang and X. Shi, *Biomaterials*, 2012, **33**, 1107-1119.
11. S. Wen, K. Li, H. Cai, Q. Chen, M. Shen, Y. Huang, C. Peng, W. Hou, M. Zhu, G. Zhang and X. Shi, *Biomaterials*, 2013, **34**, 1570-1580.
12. B. Zhou, L. Zheng, C. Peng, D. Li, J. Li, S. Wen, M. Shen, G. Zhang and X. Shi, *ACS Appl. Mater. Interfaces*, 2014, **6**, 17190-17199.
13. H. Cai, X. An, J. Cui, J. Li, S. Wen, K. Li, M. Shen, L. Zheng, G. Zhang and X. Shi, *ACS Appl. Mater. Interfaces*, 2013, **5**, 1722-1731.
14. S. Wen, Q. Zhao, X. An, J. Zhu, W. Hou, K. Li, Y. Huang, M. Shen, W. Zhu and X. Shi, *Adv. Healthcare Mater.*, 2014, **3**, 1568-1577.
15. X. Niu, H. Chen, Y. Wang, W. Wang, X. Sun and L. Chen, *ACS Appl. Mater. Interfaces*, 2014, **6**, 5152-5160.
16. F. Tang, C. Wang, J. Wang, X. Wang and L. Li, *ACS Appl. Mater. Interfaces*, 2014, **6**, 18337-18343.
17. Y. Wang, Y. Liu, H. Luehmann, X. Xia, P. Brown, C. Jarreau, M. Welch and Y. Xia, *ACS Nano*, 2012, **6**, 5880-5888.
18. C. Pérez-Campaña, V. Gómez-Vallejo, M. Puigivila, A. Martín, T. Calvo-Fernández, S. E. Moya, R. F. Ziolo, T. Reese and J. Llop, *ACS Nano*, 2013, **7**, 3498-3505.
19. R. Chakravarty, H. Hong and W. Cai, *Mol. Pharmaceutics*, 2014, **11**, 3777-3797.
20. A. de Vries, E. Custers, J. Lub, S. van den Bosch, K. Nicolay and H. Grull, *Biomaterials*, 2010, **31**, 6537-6544.
21. R. Popovtzer, A. Agrawal, N. A. Kotov, A. Popovtzer, J. Balter, T. E. Carey and R. Kopelman, *Nano Lett.*, 2008, **8**, 4593-4596.
22. M. Pérez-Hernández, P. del Pino, S. G. Mitchell, M. Moros, G. Stepien, B. Pelaz, W. J. Parak, E. M. Gálvez, J. Pardo and J. M. de la Fuente, *ACS Nano*, 2015, **9**, 52-61.
23. S. Liang, Y. Zhao, S. Xu, X. Wu, J. Chen, M. Wu and J. X. Zhao, *ACS Appl. Mater. Interfaces*, 2015, **7**, 85-93.
24. L. Guo, D. D. Yan, D. Yang, Y. Li, X. Wang, O. Zalewski, B. Yan and W. Lu, *ACS Nano*, 2014, **8**, 5670-5681.
25. M. Cheng, H. Wang, Z. Zhang, N. Li, X. Fang and S. Xu, *ACS Appl. Mater. Interfaces*, 2014, **6**, 1569-1575.
26. K. Yang, S. Zhang, G. Zhang, X. Sun, S.-T. Lee and Z. Liu, *Nano Lett.*, 2010, **10**, 3318-3323.
27. Z. Zhou, B. Kong, C. Yu, X. Shi, M. Wang, W. Liu, Y. Sun, Y. Zhang, H. Yang and S. Yang, *Sci. Rep.*, 2014, **4**, 3653.
28. T. Zhao, K. Yu, L. Li, T. Zhang, Z. Guan, N. Gao, P. Yuan, S. Li, S. Q. Yao, Q.-H. Xu and G. Q. Xu, *ACS Appl. Mater. Interfaces*, 2014, **6**, 2700-2708.
29. X. Liu, N. Huang, H. Li, H. Wang, Q. Jin and J. Ji, *ACS Appl. Mater. Interfaces*, 2014, **6**, 5657-5668.
30. Z. Zhang, C. Liu, J. Bai, C. Wu, Y. Xiao, Y. Li, J. Zheng, R. Yang and W. Tan, *ACS Appl. Mater. Interfaces*, 2015, **7**, 6211-6219.
31. R. Mooney, L. Roma, D. Zhao, D. Van Haute, E. Garcia, S. U. Kim, A. J. Annala, K. S. Aboody and J. M. Berlin, *ACS Nano*, 2014, **8**, 12450-12460.
32. Y. Xia, W. Li, C. M. Cobley, J. Chen, X. Xia, Q. Zhang, M. Yang, E. C. Cho and P. K. Brown, *Accounts Chem. Res.*, 2011, **44**, 914-924.
33. L. Gao, J. Fei, J. Zhao, H. Li, Y. Cui and J. Li, *ACS Nano*, 2012, **6**, 8030-8040.
34. Y. Wang, K. C. L. Black, H. Luehmann, W. Li, Y. Zhang, X. Cai, D. Wan, S.-Y. Liu, M. Li, P. Kim, Z.-Y. Li, L. V. Wang, Y. Liu and Y. Xia, *ACS Nano*, 2013, **7**, 2068-2077.
35. C. Sauerbeck, M. Haderlein, B. Schürer, B. Braunschweig, W. Peukert and R. N. Klupp Taylor, *ACS Nano*, 2014, **8**, 3088-3096.
36. A. Topete, M. Alatorre-Meda, P. Iglesias, E. M. Villar-Alvarez, S. Barbosa, J. A. Costoya, P. Taboada and V. Mosquera, *ACS Nano*, 2014, **8**, 2725-2738.
37. S. E. Lohse, N. D. Burrows, L. Scarabelli, L. M. Liz-Marzán and C. J. Murphy, *Chem. Mater.*, 2014, **26**, 34-43.
38. Y. I. Park, H. Im, R. Weissleder and H. Lee, *Bioconjugate Chem.*, 2015, **26**, 1470–1474.
39. H. Yuan, A. M. Fales and T. Vo-Dinh, *J. Am. Chem. Soc.*, 2012, **134**, 11358-11361.
40. J. Li, W. Wang, L. Zhao, L. Rong, S. Lan, H. Sun, H. Zhang and B. Yang, *ACS Appl. Mater. Interfaces*, 2015, **7**, 11613-11623.
41. S. Barbosa, A. Topete, M. Alatorre-Meda, E. M. Villar-Alvarez, A. Pardo, C. Alvarez-Lorenzo, A. Concheiro, P. Taboada and V. Mosquera, *J. Phy. Chem. C*, 2014, **118**, 26313-26323.
42. H. Chen, X. Zhang, S. Dai, Y. Ma, S. Cui, S. Achilefu and Y. Gu, *Theranostics*, 2013, **3**, 633-649.
43. Y. Liu, J. R. Ashton, E. J. Moding, H. Yuan, J. K. Register, A. M. Fales, J. Choi, M. J. Whitley, X. Zhao and Y. Qi, *Theranostics*, 2015, **5**, 946-960.
44. K. Lee, E. Prajatelistia, D. S. Hwang and H. Lee, *Chem. Mater.*, 2015, **27**, 6478–6481.
45. S. N. Mistry, J. Shonberg, C. J. Draper-Joyce, C. Klein Herenbrink, M. Michino, L. Shi, A. Christopoulos, B. Capuano, P. J. Scammells and J. R. Lane, *J. Med. Chem.*, 2015, **58**, 6819–6843.
46. W. Cui, M. Li, J. Liu, B. Wang, C. Zhang, L. Jiang and Q. Cheng, *ACS Nano*, 2014, **8**, 9511-9517.
47. L.-S. Lin, Z.-X. Cong, J.-B. Cao, K.-M. Ke, Q.-L. Peng, J. Gao, H.-H. Yang, G. Liu and X. Chen, *ACS Nano*, 2014, **8**, 3876-3883.
48. J. Park, T. F. Brust, H. J. Lee, S. C. Lee, V. J. Watts and Y. Yeo, *ACS Nano*, 2014, **8**, 3347-3356.
49. U. Y. Lee, Y. S. Youn, J. Park and E. S. Lee, *ACS Nano*, 2014, **8**, 12858-12865.
50. Y. Liu, K. Ai, J. Liu, M. Deng, Y. He and L. Lu, *Adv. Mater.*, 2013, **25**, 1353-1359.
51. O. Pop-Georgievski, D. Kubies, J. Zemek, N. Neykova, R. Demianchuk, E. M. Chánová, M. Šlouf, M. Houska and F. Rypáček, *Beilstein J. Nanotechnol.*, 2015, **6**, 617-631.
52. X. Liu, J. Cao, H. Li, J. Li, Q. Jin, K. Ren and J. Ji, *ACS Nano*, 2013, **7**, 9384-9395.
53. Y. Zeng, D. Zhang, M. Wu, Y. Liu, X. Zhang, L. Li, Z. Li, X. Han, X. Wei and X. Liu, *ACS Appl. Mater. Interfaces*, 2014, **6**, 14266-14277.
54. V. Ball, D. D. Frari, V. Toniazzo and D. Ruch, *J. Colloid Interface Sci.*, 2012, **386**, 366-372.
55. F. Bernsmann, V. Ball, F. Addiego, A. Ponche, M. Michel, J. J. d. A. Gracio, V. Toniazzo and D. Ruch, *Langmuir*, 2011, **27**, 2819-2825.
56. M. Lin, C. Guo, J. Li, D. Zhou, K. Liu, X. Zhang, T. Xu, H. Zhang, L. Wang and B. Yang, *ACS Appl. Mater. Interfaces*, 2014, **6**, 5860-5868.
57. Q. Tian, F. Jiang, R. Zou, Q. Liu, Z. Chen, M. Zhu, S. Yang, J. Wang, J. Wang and J. Hu, *ACS Nano*, 2011, **5**, 9761-9771.
58. O. C. Farokhzad, J. Cheng, B. A. Teply, I. S. Sherifi, S. Jon, P. W. Kantoff, J. P. Richie and R. Langer, *Proc. Natl. Acad. Sci. U. S. A.*, 2006, **103**, 6315-6320.

View Article Online
DOI: 10.1039/C6TB00773B

Figure captions

Figure 1. Schematic illustration of the synthesis and application of Au-PEI@pD NSs for theranostics of tumors.

Figure 2. UV-vis spectra of (a) Au seeds and (b) Au-PEI@pD NSs (inset of the respective panel shows the Au seeds or Au-PEI@pD NSs dispersed in water). (c) Size distribution histogram, (d) TEM image of Au-PEI@pD NSs, and (e,f) High-resolution TEM image of AuNSs-PEI and Au-PEI@pD NSs, respectively. The scale bars in each panel of (d), (e) and (f) represent 200, 20 and 50 nm, respectively.

Figure 3. (a) CT images and (b) X-ray attenuation intensity (HU) of the Au-PEI@pD NSs at different Au concentrations. (c) CT images and (d) CT values of HeLa cells treated with the Au-PEI@pD NSs at different Au concentrations for 4 h. In (d), the standard deviation is calculated *via* quantifying the CT values of cells at three different areas for each sample. CT images of the tumor region before (e) and at 10 min post intratumoral injection (f) of the Au-PEI@pD NSs ([Au] = 100 mM, in 100 μL PBS).

Figure 4. (a) Plot of temperature of water, and water solution containing the AuNSs-PEI or Au-PEI@pD NSs ([Au] = 0.35 mM for both particles) as a function of laser irradiation time. (b) Plot of temperature of water and water solution containing the Au-PEI@pD NSs at different Au concentrations (0.35, 0.7, 1.4, and 2.1 mM, respectively) as a function of laser irradiation time. (c) The temperature change (ΔT) of an aqueous solution of the Au-PEI@pD NSs as a function of Au concentration over the laser irradiation period of 300 s. (d) Plot of temperature of the aqueous solution containing the Au-PEI@pD NSs ([Au] = 2.1 mM) as a function of time (laser on for 300 s for each cycle, and laser off) for 3 cycles.

Figure 5. Thermal images of tumors after treatment with (a) PBS (0.1 mL) and (b) Au-PEI@pD NSs ([Au] = 5.6 mM, in 0.1 mL PBS), followed by irradiation with an 808 nm laser at a power density of 1.3W/cm^2. (c) The temperature change of the tumor region treated with PBS (0.1 mL) or Au-PEI@pD

NSs ([Au] = 5.6 mM, in 0.1 mL PBS) as a function of laser irradiation time.

View Article Online
DOI: 10.1039/C6TB00773B

Figure 6. Relative tumor growth volume (a), body weight (b), and survival rate (c) of HeLa tumor-bearing mice after different treatments, including the Control group (treated with PBS), NSs group (treated with the Au-PEI@pD NSs without laser), Laser group (treated with laser without the injection of the Au-PEI@pD NSs), and NSs + Laser group (treated with the Au-PEI@pD NSs and laser irradiation). In (a) and (b), the tumor-bearing mice were divided into four groups and each group contains three mice. The standard deviations of the relative tumor volume and body weight of each group were calculated on the basis of the data from three mice.

Figure 7. H&E (a) and TUNEL (b) stained micrographs of the xenografted HeLa tumor sections after different treatments. The scale bars in each panel of (a) and (b) represent 50 and 200 μm, respectively.

View Article Online
DOI: 10.1039/C6TB00773B

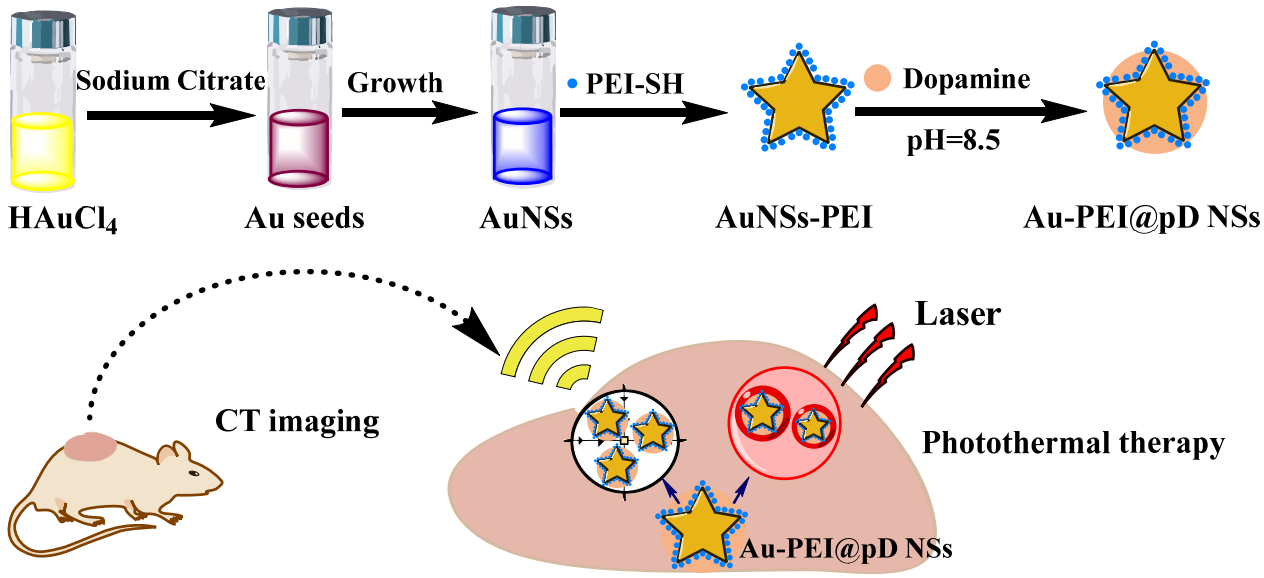

Figure 1

Li *et al.*

View Article Online
DOI: 10.1039/C6TB00773B

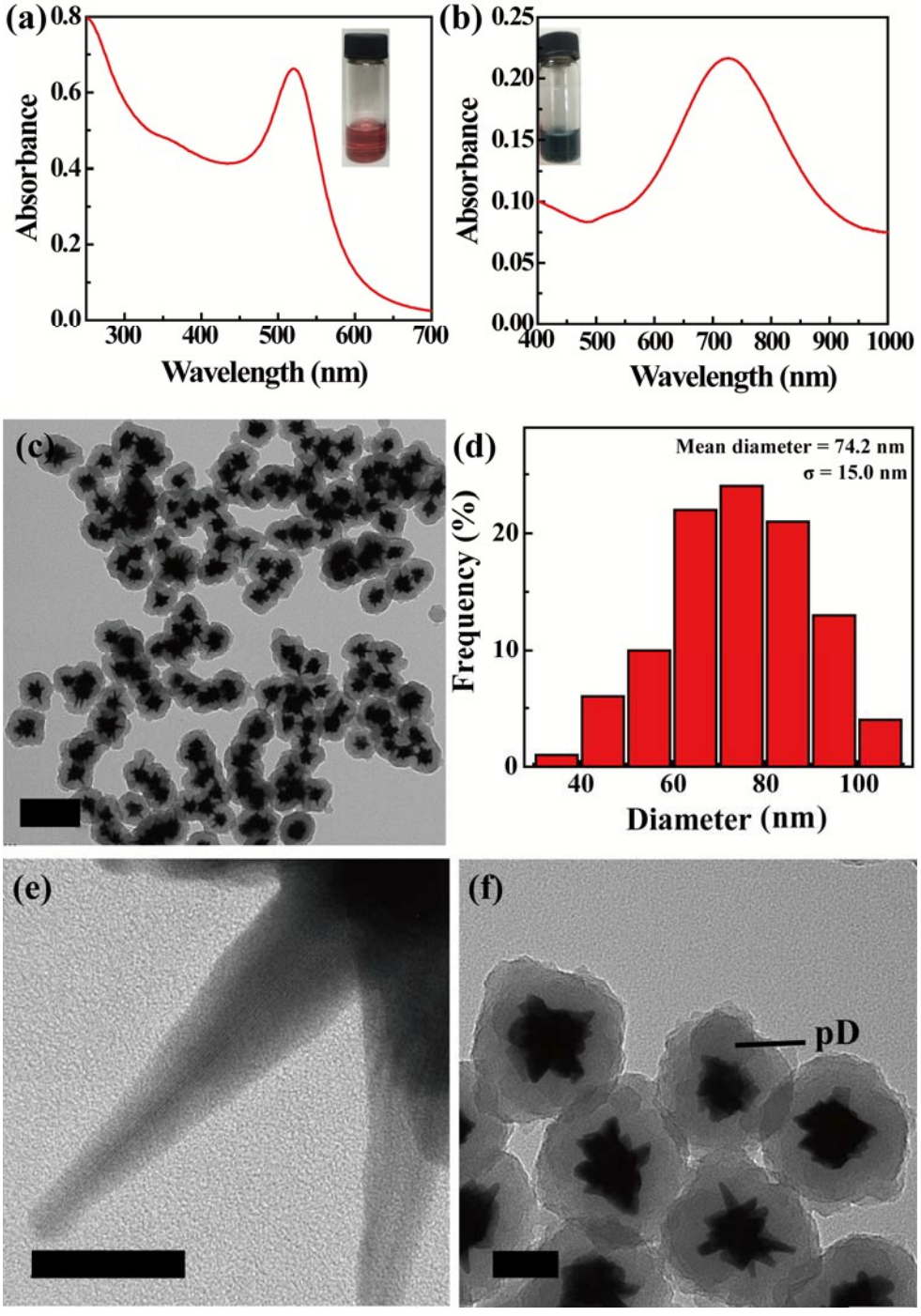

Figure 2

Li *et al.*

View Article Online
DOI: 10.1039/C6TB00773B

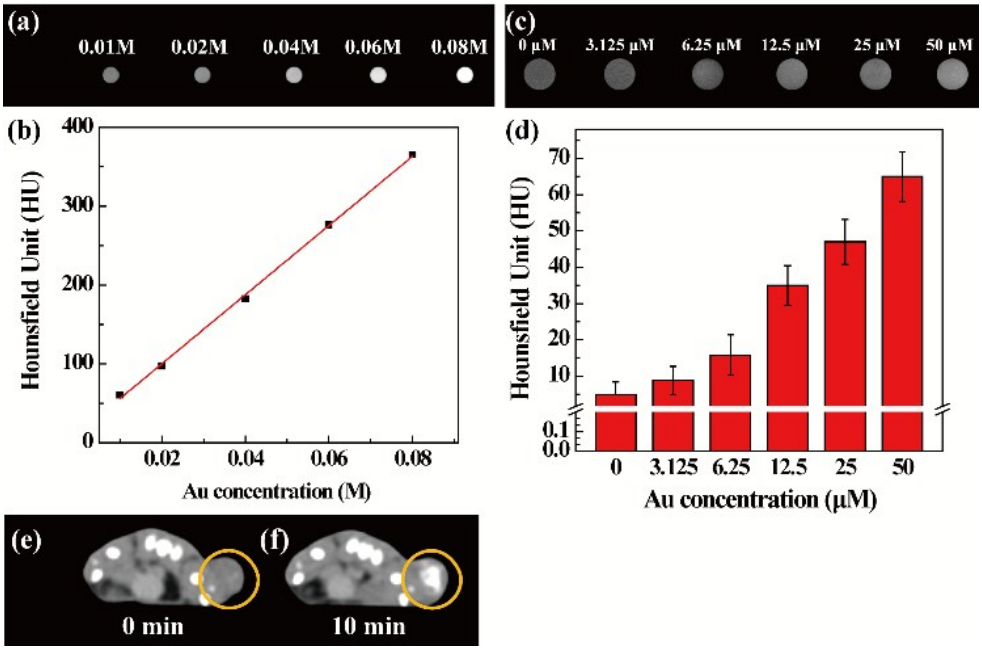

Figure 3

Li *et al.*

View Article Online
DOI: 10.1039/C6TB00773B

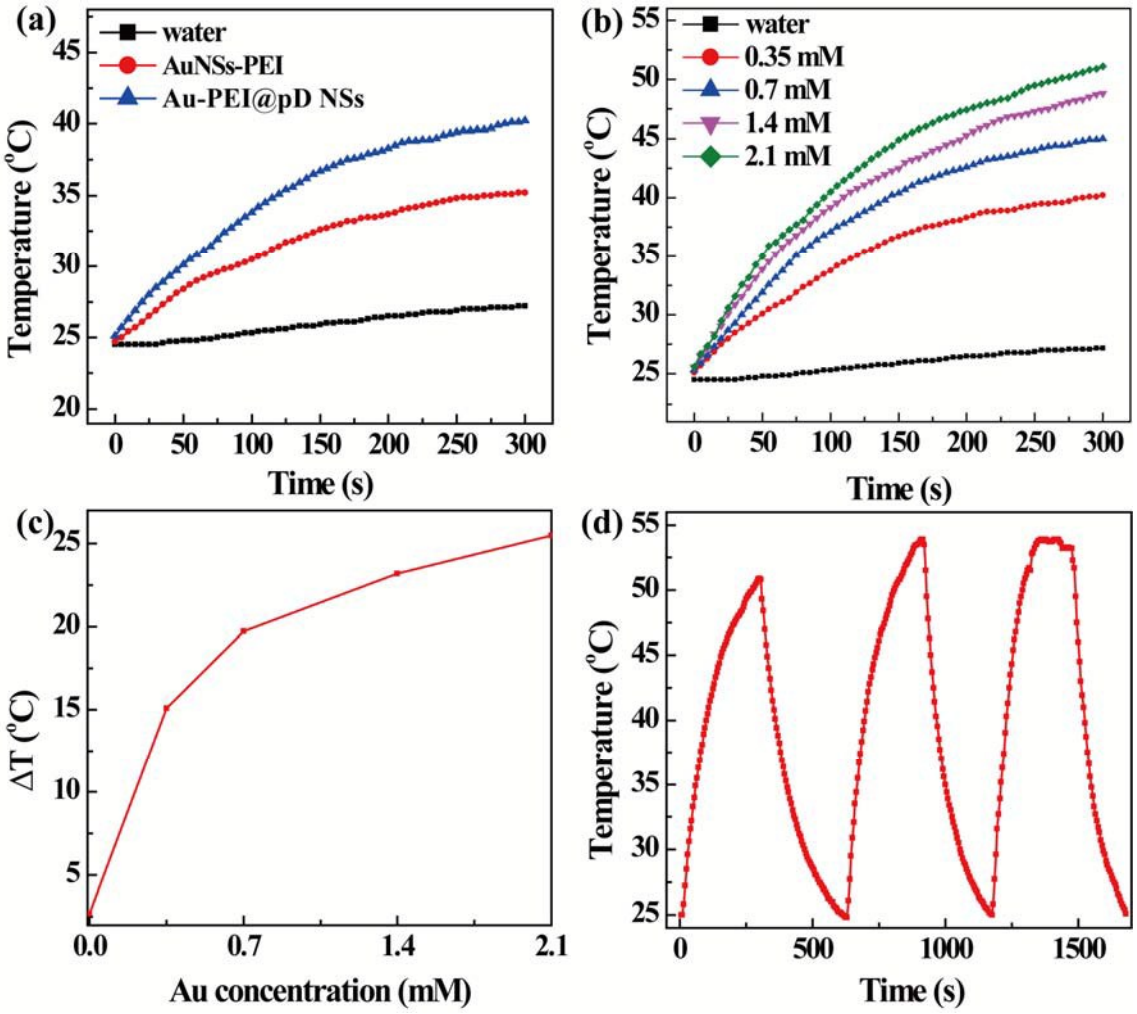

Figure 4

Li *et al.*

View Article Online
DOI: 10.1039/C6TB00773B

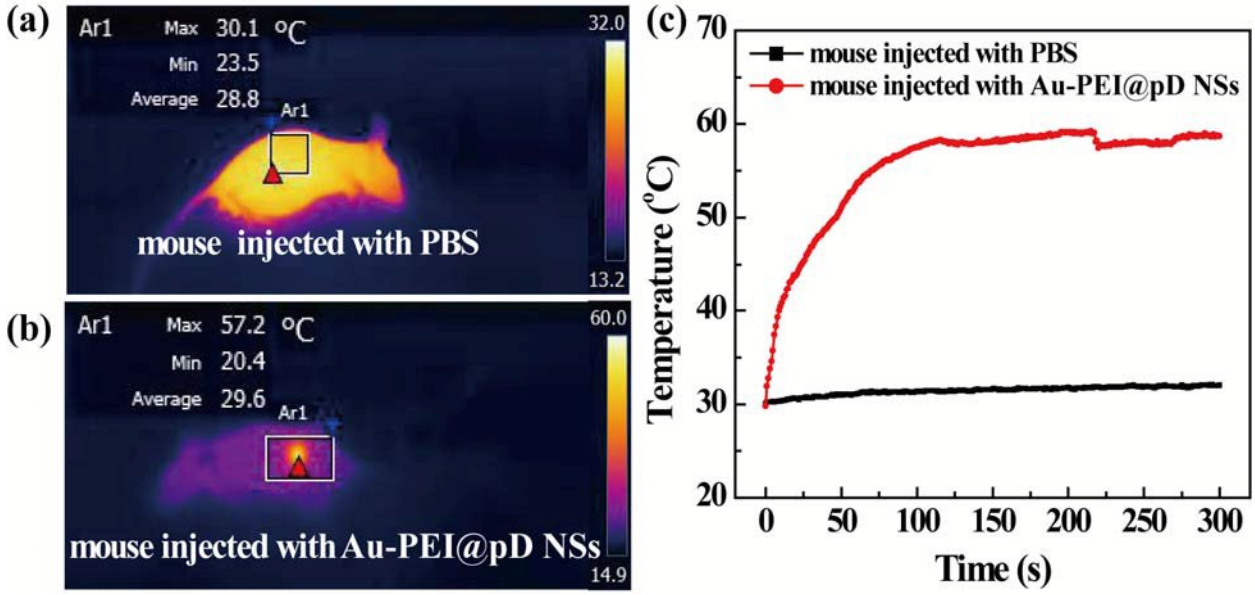

Figure 5

Li *et al.*

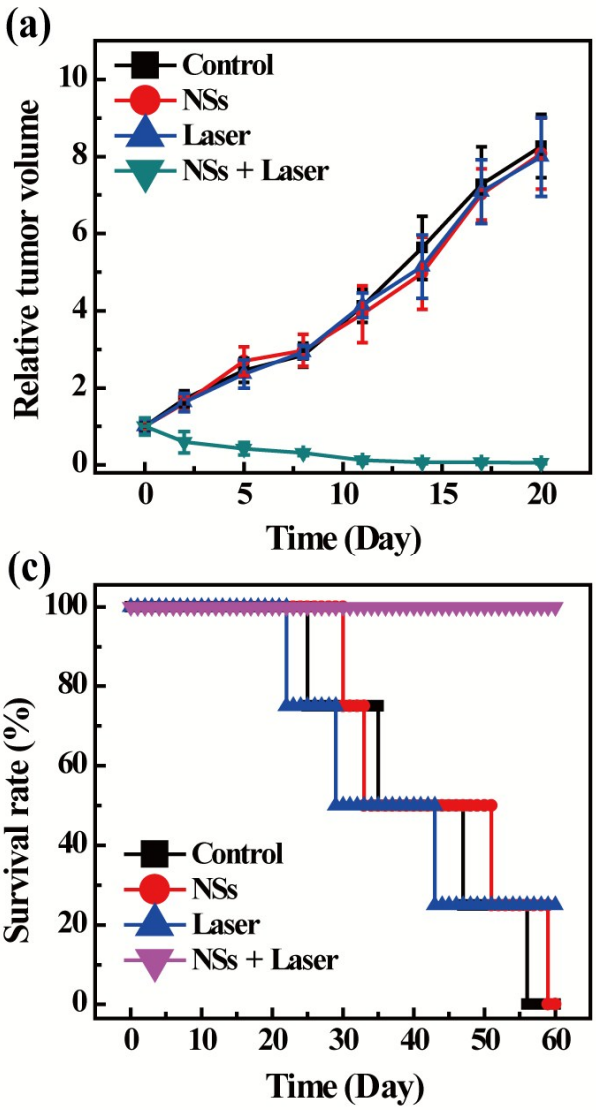

Figure 6

Li *et al.*

View Article Online
DOI: 10.1039/C6TB00773B

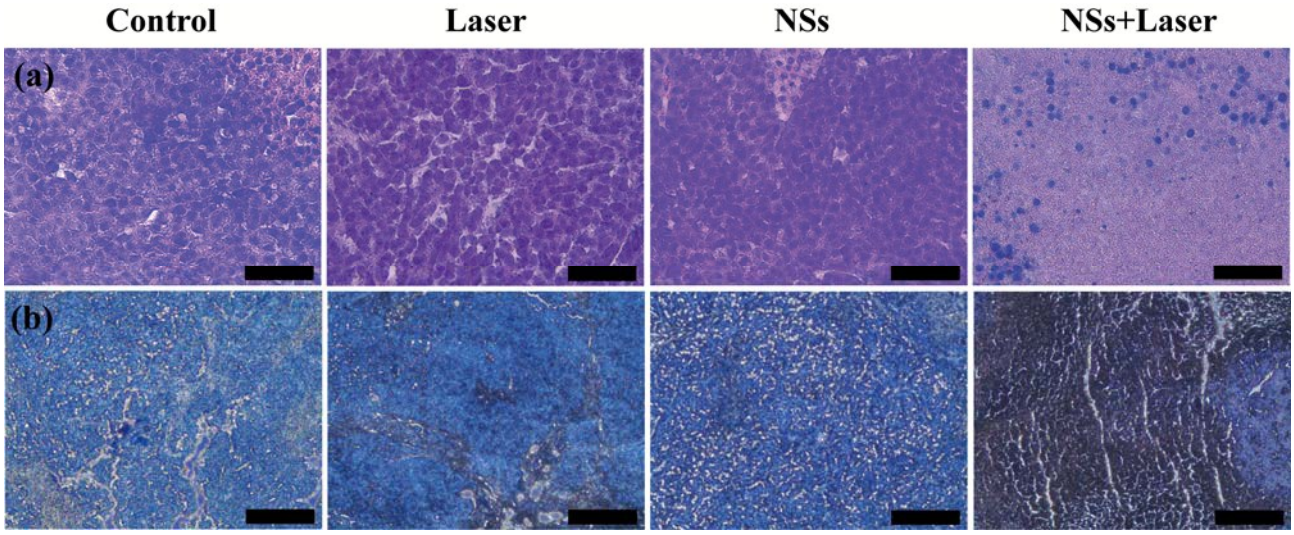

Figure 7

Li *et al.*

View Article Online
DOI: 10.1039/C6TB00773B

Table of Contents (TOC) Image

Construction of polydopamine-coated gold nanostars for CT imaging and enhanced photothermal therapy of tumors: an innovative theranostic strategy†

Du Li,[1a] Yongxing Zhang, [1b] Shihui Wen, [c] Yang Song, [c] Yueqin Tang, [d] Xiaoyue Zhu, [c] Mingwu Shen, [c] Serge Mignani, [e] Jean-Pierre Majoral, [f] Qinghua Zhao*[b] and Xiangyang Shi*[a,c]

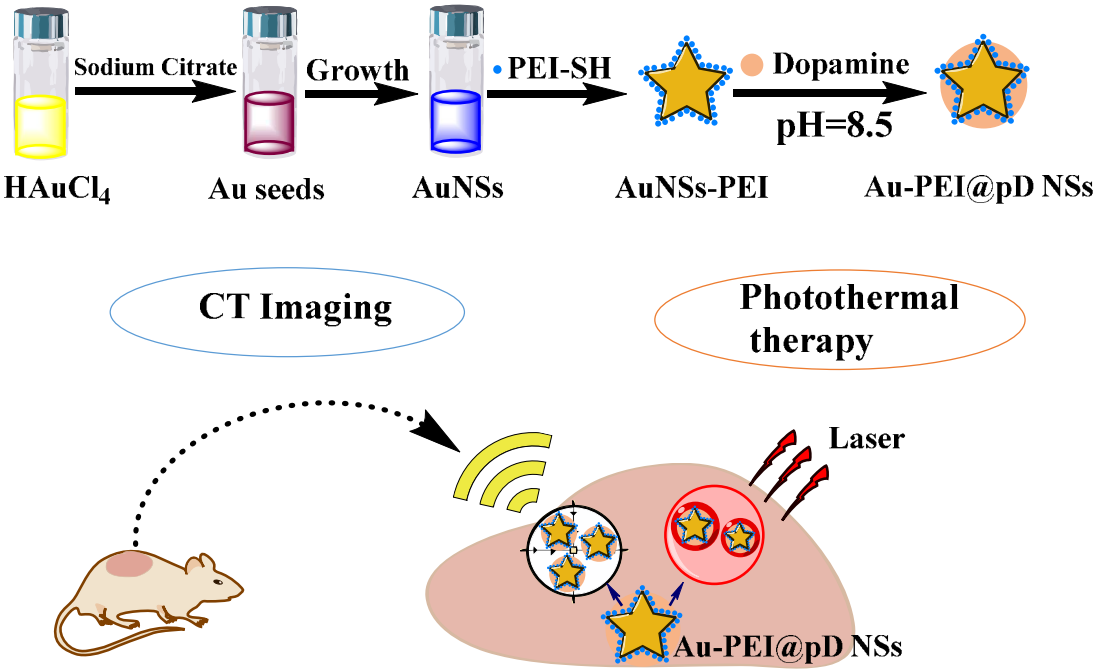

Polytheyleneimine-stabilized gold nanostars can be coated with polydopamine for computed tomography imaging and enhanced photothermal therapy of tumors.